IOP PUBLISHING PHYSICS IN MEDICINE AND BIOLOGY

Phys. Med. Biol. **53** (2008) 6195–6209 doi:10.1088/0031-9155/53/21/020

Characterization of a scintillating GEM detector with low energy x-rays

E Seravalli[1,3], M R de Boer[1], F Geurink[1], J Huizenga[1], R Kreuger[1], J M Schippers[2] and C W E van Eijk[1]

[1] Delft University of Technology, Faculty of Applied Sciences, Delft, The Netherlands
[2] Paul Scherrer Institute, Villigen, Switzerland

E-mail: e.seravalli@tudelft.nl

Received 25 July 2008, in final form 12 September 2008
Published 14 October 2008
Online at stacks.iop.org/PMB/53/6195

Abstract

A two-dimensional position-sensitive dosimetry system based on a scintillating gas detector is being developed with the aim of using it for pre-treatment verification of dose distributions in charged particle therapy. The dosimetry system consists of a chamber filled with an Ar/CF_4 scintillating gas mixture, inside which two cascaded gas electron multipliers (GEMs) are mounted. A GEM is a thin kapton foil with copper cladding structured with a regular pattern of sub-mm holes. In such a system, light quanta are emitted by the scintillating gas mixture during the electron avalanches in the GEM holes when radiation traverses the detector. The light intensity distribution is proportional to the energy deposited in the detector's sensitive volume by the beam. In the present work, we investigated the optimization of the scintillating GEM detector light yield. The light quanta are detected by means of a CCD camera or a photomultiplier tube coupled to a monochromator. The GEM charge signal is measured simultaneously. We have found that with 60 μm diameter double conical GEM holes, a brighter light signal and a higher electric signal are obtained than with 80 μm diameter holes. With an Ar + 8% CF_4 volume concentration, the highest voltage across the GEMs and the largest light and electric signals were reached. Moreover, we have found that the emission spectrum of Ar/CF_4 is independent of (1) the voltages applied across the GEMs, (2) the x-ray beam intensity and (3) the GEM hole diameter. On the other hand, the ratio of Ar to CF_4 peaks in the spectrum changes when the concentration of the latter gas is varied.

(Some figures in this article are in colour only in the electronic version)

[3] Address for correspondence: Department of Radiation, Radio Nuclides and Reactors, Delft University of Technology, Division RD&M, Mekelweg 15, 2629 JB Delft, The Netherlands.

1. Introduction

For dose verification in particle radiotherapy, we have developed a position-sensitive detector based on gas electron multipliers (GEMs) (Sauli 1997) filled with a scintillating gas mixture of Ar/CF_4. A GEM is a copper-clad thin kapton foil with a regular pattern of sub-millimetre holes. The light emitted by the electron-excited gas molecules during the gas multiplication process in the GEM holes is detected by means of a mirror-lens-CCD camera system.

When a radiation beam traverses the detector, the measured 2D light intensity distribution is proportional to the 2D distribution of the energy deposited in the detector-sensitive volume by the beam. For a measurement of a 3D dose distribution, the scintillating GEM detector can be mounted at the beam exit side of a water-bellows phantom, whose thickness is varied in steps. The combination of the high degree of granularity of the GEM holes and of the CCD camera allows imaging with sub-millimetre resolution.

Papers reporting on scintillating GEM detectors used as an imaging device have been already published (Fraga *et al* 1999, 2001a, Timmer *et al* 2002). In two recent publications (Seravalli *et al* 2007, 2008), we have shown the first results of the scintillating GEM detector for 2D dosimetry in an alpha particle beam and clinical carbon ion beam, respectively.

In the present work, we describe some of the experiments performed in an x-ray beam in our laboratory in order to optimize the detector light yield. The response of the detector is equal for x-rays and charged particles except for possible charge density effects due to the ionizations along the tracks of incoming beams. However, these effects have not been studied in this paper.

The optimization has been investigated as a function of the voltage across the GEMs, two GEM hole diameters and different Ar/CF_4 ratios. Since it is not known whether the population of excited states of the gas molecules during the multiplication process depends on the optimization parameters, we also measured the Ar/CF_4 emission spectrum for several situations. These measurements could indicate if the observed light yield changes are due to variations in the spectrum with respect to the spectral sensitivity curve of the CCD camera.

2. Methods and materials

2.1. The scintillating GEM detector

A schematic representation of the scintillating GEM detector is given in figure 1 and a detector photograph is shown in figure 2.

The detector consists of an aluminium chamber (350 mm $\times$ 350 mm $\times$ 50 mm). The 150 mm $\times$ 150 mm entrance window is made of a 25 μm thick aluminized Mylar foil. The cathode consists of a 160 mm $\times$ 160 mm 25 μm thick aluminized Mylar foil. The cathode foil is glued onto an Al frame and it is located 0.5 mm downstream of the entrance window, with respect to the radiation beam direction. Two cascaded 100 mm $\times$ 100 mm GEMs, produced at CERN (Sauli 1997), and named respectively GEM_1 and GEM_2, have been mounted. The GEMs used in this work have 80 μm (big holes) or 60 μm (small holes) diameter double conical holes with a pitch of respectively 140 μm and 90 μm, and are glued onto Al frames. The gap between the cathode and GEM_1 (drift gap) is 3.2 mm, while the gap between the two GEMs (transfer gap) is 4.2 mm. The 170 mm $\times$ 170 mm exit window is made of 3 mm thick Duran 50 glass and it is located 35 mm behind GEM_2. The exit window is made of glass with 98% transmission in the spectral sensitivity range of the CCD camera (figure 5). The cathode and GEM frames are mounted on eight support pins in the detector box. Aluminium oxide

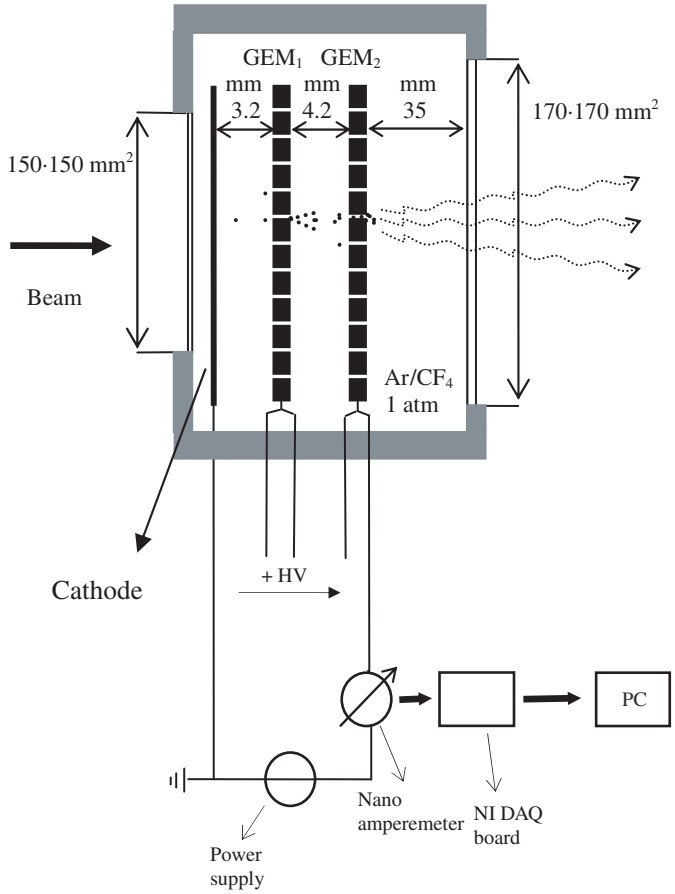

Figure 1. Schematic representation of the scintillating GEM detector set-up. The beam enters from the left side. For visualization purposes, only the nano-amperemeter of the last surface of GEM_2 is shown.

spacer rings are put around the pins in between the frames. The GEM frames are grounded to the detector box.

The detector chamber is continuously flushed with a mixture of argon and CF_4 at 9 l h^{-1} and at 1 atm. The argon normally used has a purity of 99.996% while the CF_4 has a purity of 99.998%. The two gases are mixed by means of a Brooks mixing station. The mixing station consists of two mass flow controllers (models 5850E, 5850S) and a read-out/control unit (model 5878). After mixing the two gases in the specified volumetric ratio, the gas is flushed into the detector chamber by means of 'polyflow' tubes.

The gas leaves the chamber via an oil-filled bubbler to an exhaust pipe in the experimental area. The bubbles are an indicator for the actual gas flow. The detector is used in a flow mode because we have observed that its signal output decreases when the flow rate is reduced (the light signal drops by a factor of about 19% when the flow rate is decreased by 75%) due to the presence of out-gassing materials inside the detector chamber.

A pressure sensor (Motorola MPX4115AS, case 867E, 1.5% accuracy) is used to monitor the gas pressure variations inside the detector, while the gas temperature is measured by means of a temperature sensor (precision 0.1 °C).

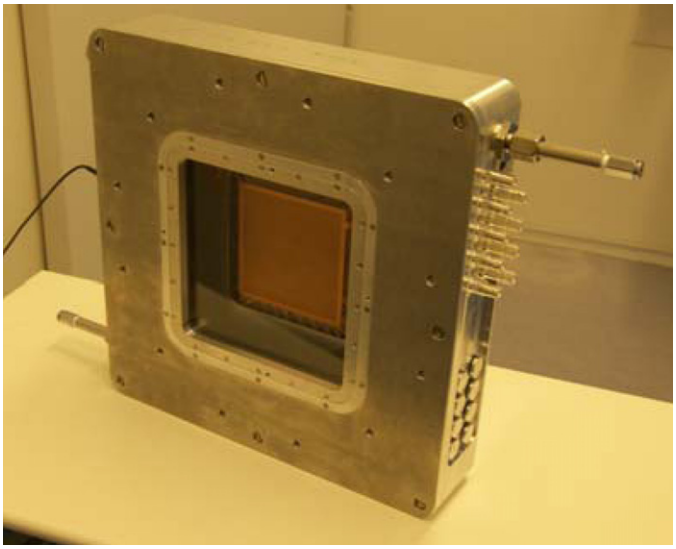

Figure 2. Exit window side of the scintillating GEM detector. Through the glass window, GEM_2 can be seen.

In presence of proper electric fields in the chamber gaps and across the GEMs, the primary electrons created in the drift gap by the incoming radiation beam drift towards the GEM_1 holes. In the GEM_1 holes, gas multiplication (avalanche) takes place. Most of the multiplied electrons drift in the electric field of the transfer gap towards GEM_2 where they are again multiplied. The electrons from the avalanche are collected on the GEM_2 surface facing the exit window. During the multiplication process, light quanta are emitted by the electron-excited Ar/CF_4 molecules when they decay to the ground state.

2.1.1. Integral light measurements. In the normal dosimetric set-up, the light quanta are detected by means of a low dark-current Apogee 1E camera coupled to a Tamron 171A zoom lens. The camera has a Kodak KAF-0401E CCD with a quantum efficiency of about 62% at ∼640 nm (figure 5). The camera is kept outside the beam to ensure low background radiation onto it. A 45° tilted mirror reflects the photons towards the camera. The distance between the detector exit window and the mirror is chosen so as to avoid reflections from the mirror back to the exit window. The light path is enclosed in a light-tight plastic tube that shields it from other light sources present in the laboratory. The CCD camera is focused on GEM_2 by means of a 100 mm diameter transparent foil with a 10 mm pitch grid which is temporarily mounted for this procedure at the GEM_2 location. The optical magnification factor of the whole set-up is 0.043, giving that 1 pixel (9 μm × 9 μm) on the CCD is equivalent to 207 μm × 207 μm at the GEM_2 position. The CCD signal per pixel is expressed in analogue-to-digital units (ADU), 1 ADU being equivalent to 8.4 electrons collected-charge on the CCD camera. During measurements, the CCD camera is cooled down to −20 °C.

Simultaneous to the light signal, the cathode and GEM currents are measured for a better understanding of the detector operation. The cathode is grounded while each GEM surface is connected to an individual channel of a positive CAEN HV power supply (SY127/A231). Nano-amperemeters, built in our electronics workshop, measure the currents flowing to the cathode and the GEM surfaces. These meters are connected in series with the supply line of

each HV channel. They have 100 kΩ impedance which yields to a precision of a few tens of nano-Amperes on the current measurement. This impedance value was chosen to have a well detectable signal and at the same time a negligible voltage drops across them (<0.5 V) for the expected beam intensities. A PC-controlled National Instruments DAQ board samples the measured currents at 1 kHz.

All experiments have been performed with drift (E_d) and transfer (E_t) fields of respectively 1 kV cm^{-1} and 1.5 kV cm^{-1}. These values correspond to the optimal ones giving the best light yield. They were found to be identical for small and big hole GEMs.

2.1.2. Emission spectrum measurement set-up. For the emission spectrum measurements, the Ar/CF_4 light emitted under irradiation was analysed by a Macam monochromator (mod. MCG 910) equipped with a 1200 grooves mm^{-1} grating (8 nm mm^{-1} dispersion and about 3.5 nm resolution) and recorded by means of a Hamamatsu R943-02 photomultiplier tube covering the wavelength region 250–850 nm. The photomultiplier tube was supplied with −1700 V, cooled down to −20 °C and operated in a counting mode. It has a quantum efficiency of about 14% at 633 nm (Hamamatsu 2008). The monochromator coupled to the photomultiplier was installed behind the mirror. The light path from the scintillating GEM detector to the photomultiplier tube was properly shielded in order to avoid ambient light contamination.

The emission spectra reported in the following are corrected for the sensitivity of the set-up. The sensitivity curve was measured by means of a calibrated EPLAB 1000 Watt Quartz Iodine Lamp. A high-pass filter was not placed at the entrance slit of the monochromator for eliminating second-order diffraction effects because negligible differences were found between two spectra measured with and without a filter with 435 nm cut-off wavelength.

The current flowing on the GEM_2 surface facing the exit window is fed in this case to a current-to-voltage converter. A voltage-to-frequency converter converts the resulting voltage into a pulsed signal that is counted by the same electronics used to count the photomultiplier signal. The frequency of these pulses is proportional to the voltage. By counting the pulses during a certain time interval, we obtain a measurement of the charge during that time.

2.2. The irradiation set-up

Measurements were performed in an x-ray beam produced by an x-ray generator with a copper anode. The x-ray generator high voltage and current settings were set during the experiments in the ranges 12–24 kV and 0.75–15 mA, respectively. As can be seen in figure 3, the scintillating GEM detector was positioned, with the entrance window facing the x-ray generator, downstream of a 3 cm diameter collimator.

For every single integral light measurement, the beam is turned on for 30 s. In that period, a number of x-rays are delivered to the scintillating GEM detector. The CCD camera shutter is opened and the light emitted during the beam on time is collected on the CCD. The GEM detector electric signals are sampled simultaneously.

For the emission spectrum measurements, the beam is switched on for a long period (∼960 s). During this period the monochromator makes every 4 s a step of 2 nm covering the wavelength region 400–820 nm. This wavelength range was chosen by taking into account the sensitivity of the CCD camera (because this is normally used as readout). The photomultiplier signal is integrated over each wavelength step and then counted. Simultaneously, the current flowing on the GEM_2 surface facing the exit window is integrated every 4 s for each wavelength step.

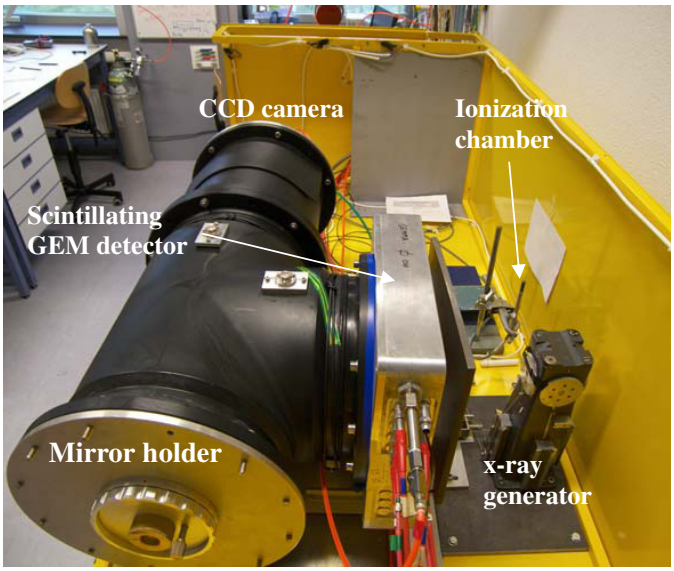

Figure 3. The irradiation setup.

During the experiments, the output of the x-ray generator is constantly monitored by means of a PTW ionization chamber (0.69 cm^3) positioned in front of another beam port whose shutter works synchronously with respect to that used to irradiate the scintillating GEM detector. The integrated signal of this ionization chamber is named q-Ic.

2.3. Quantities

The CCD camera pictures are processed offline using Matlab routines. The CCD camera dark current is compensated for by subtracting a so-called *background picture*. This *background picture* is recorded for the same exposure time as the normal picture, with the beam off and camera shutter open. The integrated light yield, L_i, has been calculated by integrating the background-corrected picture pixel values in ADU over a circular region of interest. The region of interest is chosen bigger than the beam spot in the pictures and it is kept constant for all the pictures.

We define as output current, I_{out}, the current flowing to the surface of GEM_2 facing the exit window. The I_{out} offset, $\langle I_{\mathrm{offset}}\rangle$, is calculated by taking the mean value over $N_1 = 2000$ samples of $I_{\mathrm{out}}(t_i)$ recorded before the beam starts (t_{s}).

The output charge q_{out} is evaluated by summing the offset-corrected I_{out} values between t_{s} and t_{f} (beam stops) instants. Between t_{s} and t_{f} instants, N_2 samples are measured. Δt is the sampling time, 1 ms:

$$q_{\mathrm{out}} = \left(\sum_{i=\mathrm{s}}^{i=\mathrm{f}} (I_{\mathrm{out}}(t_i) - \langle I_{\mathrm{offset}}\rangle)\right) \cdot \Delta t \qquad \text{with} \quad t_{\mathrm{s}} < t_{\mathrm{f}}. \tag{1}$$

In the following, L_{i} and q_{out} are normalized to the integrated signal of the PTW ionization chamber, q-Ic.

We define the light production efficiency Y as the ratio of L_i to q_{out} ($Y = L_i/q_{\mathrm{out}}$). Y is a measure for the efficiency of the light production in the avalanches (Fraga *et al* 2002a) since

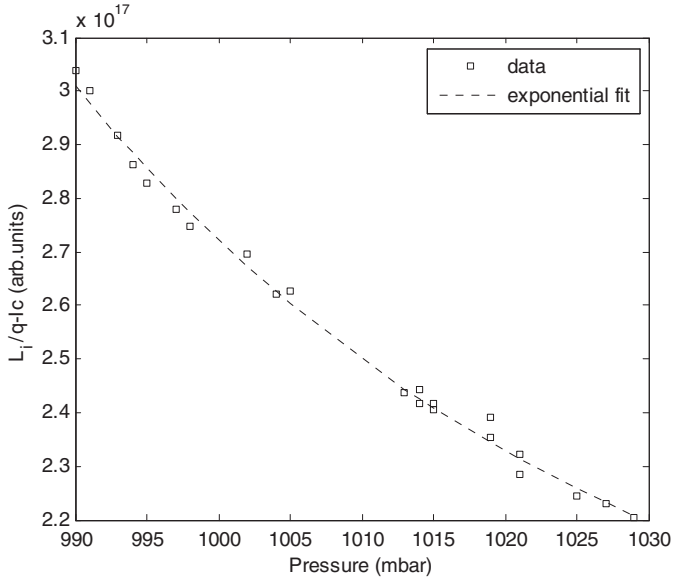

Figure 4. Correlation plot of L_i and the pressure. The exponential fit, $A + B \cdot e^{-\frac{p}{C}}$, is also represented.

now the light yield is normalized to the number of electrons produced during these avalanches. Therefore, this is a good quantity to compare the light production efficiency for scintillating GEM detector set-ups with different charge gains (i.e. ratio of q_{out} to the primary electrons created in the drift gap by the radiation beam).

The counts recorded by means of the photomultiplier are compensated for the photomultiplier background counts evaluated before the x-ray beam starts. The GEM detector light and electric counted signals are respectively defined as *light-counted* and q_{out}-*counted*. In this case, Y is calculated as the ratio of the light-counted to the corresponding q_{out}-counted. In the following, the counted signals are normalized to q-Ic as well.

2.4. Pressure correction

In the following, the detector outputs have been corrected for atmospheric pressure variations. For example, L_i pressure corrected, L_i^c, is defined as

$$L_i^c = f \cdot L_i \qquad \text{and} \qquad f = \frac{A + B \cdot e^{-\frac{p_{\text{ref}}}{C}}}{A + B \cdot e^{-\frac{p}{C}}}, \tag{2}$$

where p_{ref} is the pressure value taken as a reference, p is the atmospheric pressure value at which the experiment is performed and A, B, C are fit parameters determined by fitting the exponential function $A + B \cdot e^{-\frac{p}{C}}$ to the data plotted in figure 4. This type of fit was chosen according to the data trend and it is not based on a physical model. It is only used to calculate intermediate points in the graph of figure 4.

The calibration curve shown in figure 4 was performed by varying the pressure inside the detector by means of adjusting a needle valve inserted in series to the exhaust gas tube between the detector chamber and the glass bubbler. For each pressure value, L_i was recorded. The pressure was varied in the interval 990–1028 mbar because it was observed that the

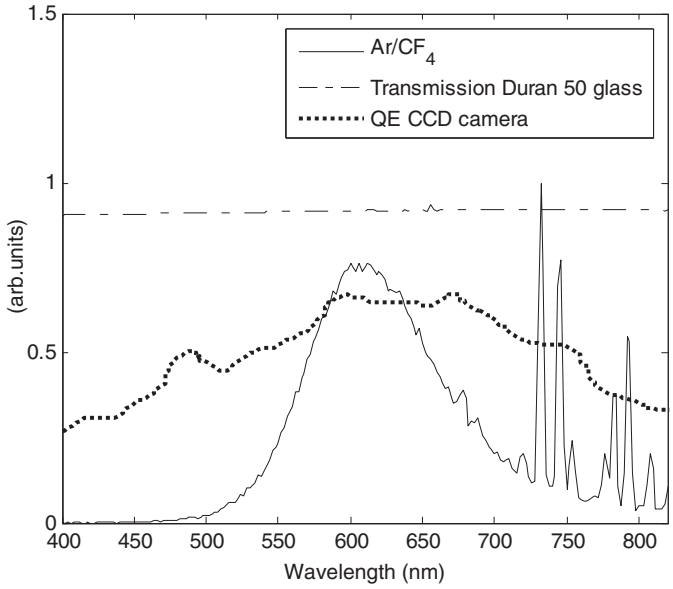

Figure 5. Emission spectrum of Ar + 8% CF_4 normalized to the highest light intensity value (solid line) graphed together with exit window Duran 50 glass transmission (dashed-dot line) and the CCD camera quantum efficiency (QE) (dot line).

atmospheric pressure in the laboratory and so inside the detector was on average changing within this range.

The uncertainty introduced by the pressure correction of L_i was evaluated by comparing integrated light yield values corrected with two independently measured calibration curves. It was found that the biggest difference between two L_i pressure-corrected values was about 1.3%.

In the same way, the pressure-corrected q_{out}, q^c_{out}, is defined. The counted signals were compensated for pressure variations as well.

We did not compensate the detector outputs for temperature variations because the temperature was constant in the laboratory when the measurements were performed.

3. Results and discussion

3.1. The Ar/CF_4 emission spectrum

In figure 5, the Ar + 8% CF_4 emission spectrum measured for small hole GEMs with voltages across GEM_1 and GEM_2 $\Delta V_{\text{GEM1}} = \Delta V_{\text{GEM2}} = 425$ V in the wavelength interval 400–820 nm is shown together with the transmission of the exit window glass and the CCD camera quantum efficiency (QE). The spectrum is characterized by a broad band with a maximum of intensity around 620 nm, and by several sharp lines between 720 and 820 nm. The shape of the measured spectrum is in agreement with the spectrum presented in Fraga *et al* (2003). According to Fraga *et al* (2003), the broad band in the visible region results from the excitation of a Rydberg state of the CF_4 molecule (CF_3^*) that dissociates into an emitting CF_3 fragment. The sharp spectral lines are attributed to excited states of Ar. For more details, see references within that article.

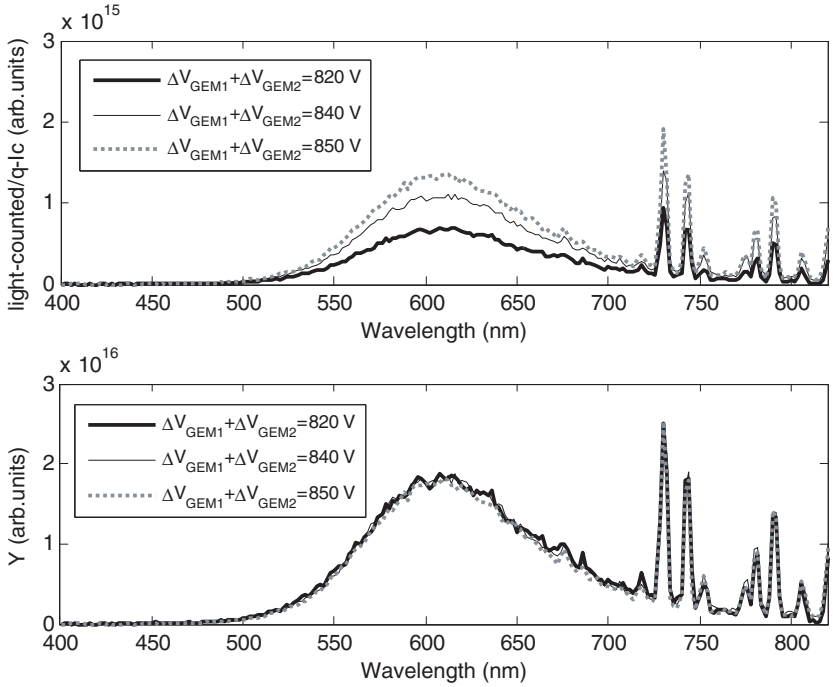

Figure 6. Small-hole GEMs' Ar + 8% CF_4 emission spectrum as a function of the voltage supplied across the GEMs, with $\Delta V_{GEM1} = \Delta V_{GEM2}$. Top graph: on the *y*-axis, the light-counted signal is represented. Bottom graph: on the y-axis, *Y* is represented.

The Ar/CF_4 emission spectrum also has a band in the UV region (Fraga *et al* 2003), but this spectral region was not of interest for this work since the QE of the Kodak KAF-0401E CCD is zero in the UV range. In fact, the QE of the CCD matches quite well the Ar/CF_4 emission spectrum: the QE has a maximum of about 62% at ∼640 nm, the wavelength for which Ar/CF_4 also has a maximum (figure 5).

3.1.1. Ar/CF_4 emission spectrum as a function of GEM voltages. The small hole GEMs' Ar + 8% CF_4 emission spectrum shape is independent of the voltage across the GEMs, with $\Delta V_{GEM1} = \Delta V_{GEM2}$, as can be seen in the upper graph of figure 6. The spectrum area increases with the voltage, because when the voltage is increased, the gain of the detector becomes higher and so more light is emitted. If the emission spectrum is expressed in terms of *Y*, its area does not change if the voltage is increased (lower graph of figure 6). This means that the spectral emission and the light production efficiency do not depend on the GEM voltage.

3.1.2. Ar/CF_4 emission spectrum as a function of x-ray intensity. We measured small hole GEMs' Ar + 8% CF_4 spectra for three different x-ray tube currents, keeping the voltage difference across the small hole GEMs fixed. No significant differences were observed among the three spectra measured with 10, 15 and 20 mA x-ray tube current and 24 kV.[4] This

[4] These x-ray tube settings correspond to a photon flux of respectively 1.4×10^9, 2.04×10^9 and 2.7×10^9 photons $cm^{-2}\ s^{-1}$.

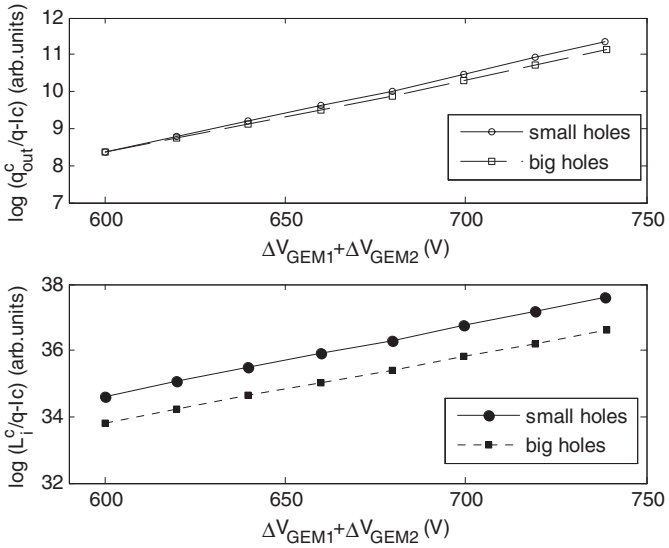

Figure 7. q^c_{out} (top graph) and L^c_i (bottom graph) as a function of $\Delta V_{\text{GEM1}} + \Delta V_{\text{GEM2}}$ measured for GEMs having small and big holes in Ar + 6% CF_4.

indicates that there is no saturation of the light production process for beam rates up to 2.7 $\times$ 10^9 photons $\text{cm}^{-2}\ \text{s}^{-1}$.

3.2. GEM hole size

3.2.1. Integral light measurements. We investigated the response of the detector as a function of the GEM hole size and pitch. q_{out} and L_i were measured for GEMs having small and big holes (section 2.1) in Ar + 6% CF_4 as a function of $(\Delta V_{\text{GEM1}} + \Delta V_{\text{GEM2}})$ with $\Delta V_{\text{GEM1}} = \Delta V_{\text{GEM2}}$. The voltage across the GEMs was increased till the maximum operating GEM voltage[5] was reached.

It can be seen in the upper graph of figure 7 that the electric and light signals increase if the voltage across the GEMs is increased, as already observed in the top graph of figure 6.

At larger $(\Delta V_{\text{GEM1}} + \Delta V_{\text{GEM2}})$ values, q_{out} measured with GEMs having small holes is slightly higher than q_{out} measured for big holes. A gain increase of the same order of magnitude for small hole GEMs is also observed in figure 13 of Bachmann *et al* (1999).

The difference in L_i values is higher than the q_{out} difference and it is independent of the voltages supplied across the GEMs, as shown in the lower graph of figure 7.

In table 1, q^c_{out}, L^c_i and Y for small and big holes are summarized for data measured at $(\Delta V_{\text{GEM1}} + \Delta V_{\text{GEM2}}) = 739$ V.

3.2.2. Ar/CF_4 emission spectrum. We measured small hole and big hole GEMs' Ar + 8% CF_4 spectrum with $(\Delta V_{\text{GEM1}} + \Delta V_{\text{GEM2}}) = 850\ V$ and $\Delta V_{\text{GEM1}} = \Delta V_{\text{GEM2}}$ in both cases. No significant differences were observed between the shapes of the two spectra when expressed in terms of light-counted and Y.

[5] The maximum operational voltage is defined here as the GEM voltage above which the GEM is in a steady discharge mode or the power supply 'trips' because of an over current.

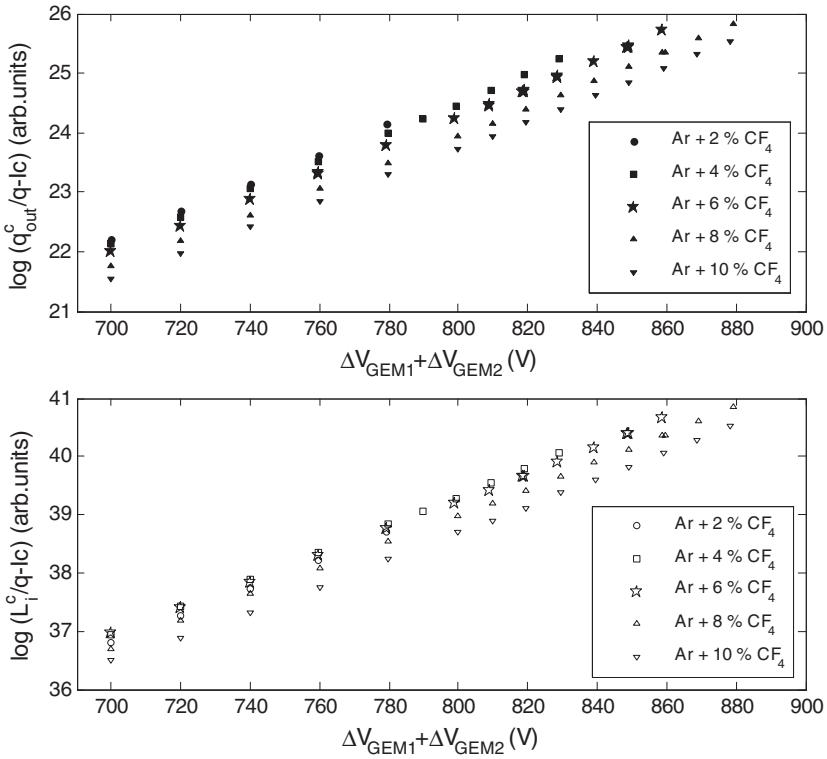

Figure 8. $q^c_{\rm out}$ (top graph) and L^c_i (bottom graph) as a function of the sum of the voltages applied to GEM_1 and GEM_2, with $\Delta V_{GEM1} = \Delta V_{GEM2}$ for Ar + x% CF_4 with $x = 2, 4, 6, 8, 10$. The data are for small-hole GEMs.

Table 1. Output charge $q^c_{\rm out}$, integrated light yield L^c_i, and light production efficiency Y measured for GEMs having small and big holes at $(\Delta V_{GEM1} + \Delta V_{GEM2}) = 739$ V in Ar + 6% CF_4.

	$q^c_{\rm out}$/q − Ic (arb. units)	L^c_i/q − Ic (arb. units)	Y (ADU/C)
Small holes	$(8.62 \pm 0.17) \times 10^4$	$(2.19 \pm 0.05) \times 10^{16}$	$(2.54 \pm 0.07) \times 10^{11}$
Big holes	$(6.84 \pm 0.13) \times 10^4$	$(0.80 \pm 0.02) \times 10^{16}$	$(1.17 \pm 0.03) \times 10^{11}$
Ratio	1.26	2.74	2.17

3.2.3. Discussion. Table 1 shows that the light yield is 2.7 times larger for small hole GEMs and the light production efficiency for this type of hole is a factor of 2.17 higher than that of big holes. In Fraga *et al* (2002b), a similar effect has been found with a He/CF_4 gas mixture.

GEMs with small holes have a ∼1.4 higher optical transparency (open-to-total GEM area ratio) and so a better electron collection efficiency[6] compared to big hole GEMs (Bachmann *et al* 1999).

Consequently, a greater number of electrons is focused on the holes. So with equal gain, higher $q_{\rm out}$ is obtained. In addition to that, the electric field strength is stronger in the centre of the small holes (Bachmann *et al* 1999). Because the Ar and CF_4 ionization probability

[6] The electron collection efficiency is defined as the ratio of electrons collected into the GEM holes to the number of arriving electrons (Killenberg *et al* 2003).

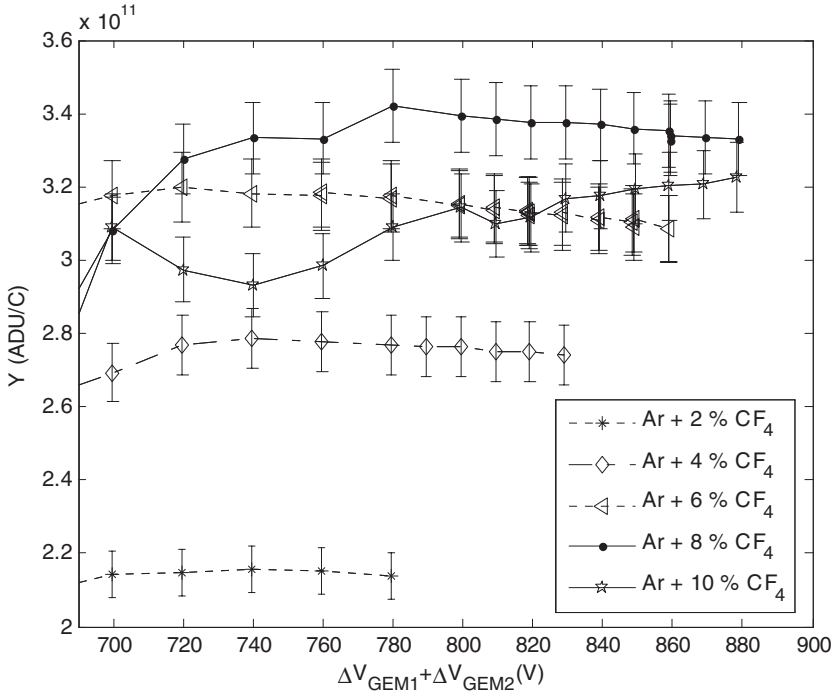

Figure 9. Y as a function of the small-hole GEMs' voltage measured for Ar + x% CF_4 with $x = 2$, 4, 6, 8, 10.

increases with the electric field intensity, more electrons are produced in the multiplication process (higher gain) as well. So, a higher number of electrons (q_{out}) explains in part (factor 1.26 in table 1) a larger light yield for small hole GEMs since L_i is linearly related to q_{out} (Seravalli *et al* 2007).

Another reason for the increased light yield is the higher light production efficiency in small-hole GEMs. However, the larger Y measured with small-hole GEMs cannot be attributed to a change in the emission spectrum shape since its shape is independent of the hole diameter (section 3.2.2). The fact that for small holes Y is larger than that for big holes must be related to the excitation probability. The hole size affects not only the field strength, but also the field configuration (Bachmann *et al* 1999). The distribution of strong and weaker electric field regions, as encountered by the traversing electrons, may play a role since the cross-sections for excitation and ionization have a different field strength dependence (Seravalli 2008). If the excitation of Ar and CF_4 is more probable than their ionization in small-hole field configurations, then more light quanta could be produced with respect to the electrons. Further studies are needed to better understand this subject.

3.3. Ar/CF_4 ratio

3.3.1. Integral light measurements. The gas mixtures Ar + x% CF_4 with $x = 2$, 4, 6, 8 or 10 were investigated for small-hole GEMs. For each Ar and CF_4 ratio, q_{out} and L_i were recorded as a function of the sum of GEM voltages with $\Delta V_{\text{GEM1}} = \Delta V_{\text{GEM2}}$. The latter were increased till the maximum operating GEM voltage was reached.

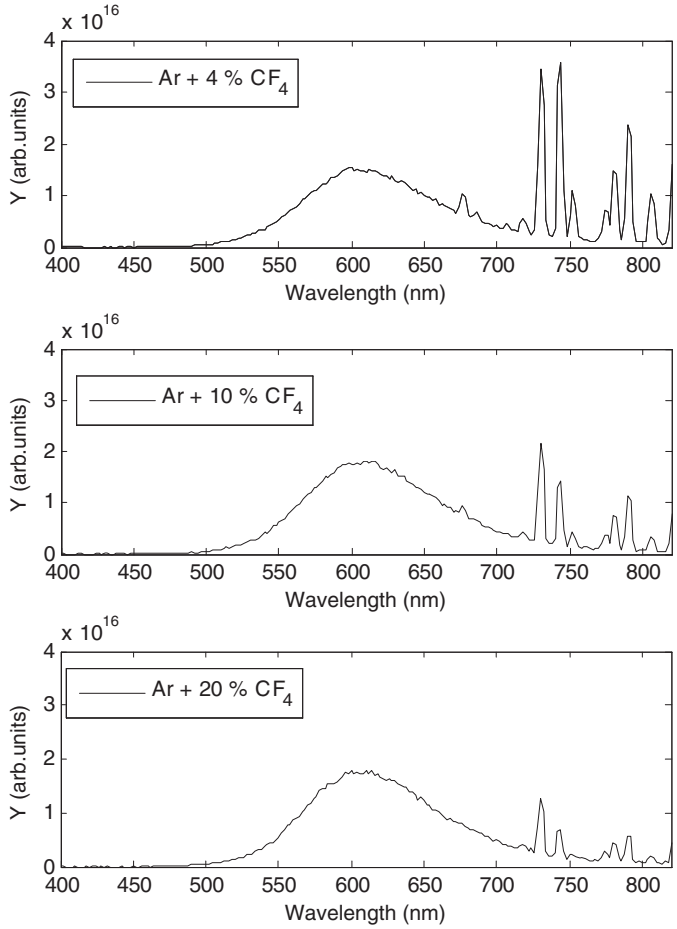

Figure 10. Emission spectra measured for small-hole GEMs in Ar + 4% CF_4, Ar + 10% CF_4 and Ar + 20% CF_4. On the *y*-axis, the light efficiency is reported.

In the upper graph of figure 8, the q^c_{out} amplification curves for the gas mixtures mentioned above are represented. The highest maximum operational GEM voltage is reached in Ar + 8 or 10% CF_4. These curves are in agreement with, for example, figure 1 of Deptuch and Kowalski (2007).

In the lower graph of figure 8, L^c_i amplification curves are shown. For a fixed (ΔV_{GEM1} + ΔV_{GEM2}), for example 819 V, L^c_i decreases when the CF_4 concentration increases from 4% to 10%. The same can be concluded for q^c_{out}. The highest L^c_i value is measured for Ar + 8% CF_4, at the highest maximum operational GEM voltage.

Figure 9 represents Y as a function of (ΔV_{GEM1} + ΔV_{GEM2}) for the different gas mixtures investigated. For a fixed Ar + x% CF_4 mixture, Y is in first approximation independent of the GEM voltage as already seen in figure 6. Also in Fraga *et al* (2001b), it is shown that the number of light quanta normalized to q_{out} is independent of the detector gas gain. Y increases when the CF_4 concentration increases from 2 to 8%. For the latter concentration, Y is at maximum. Concluding, Ar + 8% CF_4 allows reaching the highest stable GEM operational voltage, which corresponds to the highest q_{out}, the brightest L_i and the largest Y.

3.3.2. Emission spectra. In figure 10, an Ar + 4% CF_4 light production efficiency spectrum is compared to Ar + 10% CF_4 and Ar + 20% CF_4 spectra. The spectra were collected for small-hole GEMs and $\Delta V_{GEM1} = \Delta V_{GEM2}$. It is clearly visible that the intensity of the Ar atomic lines decreases when the percentage of CF_4 increases from 4 to 20%. In fact, CF_4 is a quencher gas that absorbs the photons emitted by the noble gas.

On the other hand, the height of the CF_4 visible broad band slightly increases (by a factor of ∼11%) when the CF_4 concentration is varied from 4% to 20% CF_4. According to Fraga *et al* (2003), the fact that even for small CF_4 concentrations the height of the CF_4 visible broad band is comparable to that measured for higher concentrations suggests that the direct excitation of CF_4 molecules by electron impact is not the only channel leading to the CF_3^* emission. An energy transfer mechanism between the excited states of argon and the dissociative electronic excited states of CF_4 may be present.

The integral of the light production efficiency spectrum increases by about 14% when the CF_4 concentration increases from 4% to 10%. The increase is of the same order of magnitude as that found for the same CF_4 concentrations with the integral light measurements shown in figure 10. This indicates that for these CF_4 concentrations while the Ar line intensity decreases, the CF_4 emission increases and that the measured Y increase between Ar + 4% CF_4 and Ar + 10% CF_4 is due to the increased CF_4 concentration.

The differences between the top and bottom graphs of figure 10 are similar to the differences visible in the two spectra of figure 2 of Fraga *et al* (2003), measured respectively for Ar + 5% CF_4 and Ar + 67% CF_4. In figure 10, the quenching of the Ar lines for a CF_4 concentration increase from 4 to 20% is higher than the quenching of the same lines reported in figure 2 of Fraga *et al* (2003), where the CF_4 concentration increased from 5 to 67%. This effect could be caused by the presence of some air inside the scintillating GEM detector chamber, which acts as a quencher reducing the Ar emission.

4. Conclusions

We have developed a scintillating gas detector, equipped with two cascaded GEMs in an Ar/CF_4 gas mixture in view of 2D dosimetry applications in particle therapy. In this work, we report on the characterization of the scintillating GEM detector in an x-ray beam. The aim of the characterization was to better understand the optimization of the detector light signal as a function of the voltage across the GEMs, the GEM hole size and the Ar/CF_4 ratio.

In the normal dosimetry set-up, the light quanta emitted by the Ar/CF_4 electron-excited molecules in the gas multiplication process are detected by a CCD camera. For emission spectrum measurements, the CCD camera is replaced by a photomultiplier tube coupled to a monochromator. Simultaneous to the light signal, GEM currents are also measured for a better understanding of the detector operation.

We have found that the shape of the measured Ar/CF_4 light emission spectrum is in agreement with that reported in the literature. The CCD camera sensitivity matches well the emission spectrum. Furthermore, we found that the shape of the Ar/CF_4 emission spectrum is independent of (1) the voltages applied across the GEMs, (2) the x-ray beam intensity in the range (1.4–2.7) × 10^9 photons cm^{-2} s^{-1} and (3) the GEM hole diameter. The ratio of CF_4 and Ar contributions to the spectrum area changed when their concentrations were varied.

With 60 μm diameter GEM holes (small holes), a brighter light signal and a higher electric output are measured than with 80 μm diameter holes (big holes). Part of the larger light yield recorded with small holes is related to the higher number of electrons that contribute to the light quanta production process. The higher number of electrons is due to a better electron

collection efficiency, which allows a higher number of electrons to be focused on the small holes, and to a stronger electric field configuration along the hole axis.

Another reason for the increased light yield is a better light production efficiency in small-hole GEMs. The fact that the production of light quanta is more efficient in small holes is probably related to the excitation probability. The distribution of strong and weaker electric field regions, as encountered by the traversing electrons, is different for the two hole dimensions. The cross-sections for excitation and ionization have a different field strength dependence. If now the excitation of Ar and CF_4 is more probable than their ionization, then more light photons could be produced with respect to the electrons.

By varying the CF_4 concentration, it was found that Ar + 8% CF_4 volume percentage allowed reaching the highest voltage across the GEMs and the highest detector light output.

For future dosimetry tests of this detector, we will use small-hole GEMs and Ar + 8% CF_4 in order to have the largest light signal and hence a better SNR in the CCD camera.

Acknowledgments

We thank Dr M Fraga and Professor F Fraga for interesting and fruitful discussions and Dr J Jansen, Dr G Bizarri and J de Haas for having helped in setting up some of the experiments and their availability. This work was supported by the Foundation for Fundamental Research on Matter (FOM).

References

Bachmann S, Bressan A, Ropelewski L, Sauli F, Sharma A and Mörmann D 1999 Charge amplification and transfer processes in the gas electron multiplier *Nucl. Instrum. Methods* A **438** 376–408

Deptuch M and Kowalski T Z 2007 Gas multiplication process in mixtures based on Ar, CO_2, CF_4 *Nucl. Instrum. Methods* A **572** 184–6

Fraga F A F, Fetal S T G, Margato L M S, Ivaniouchenkov I, Marques R F and Policarpo A J P L 1999 Imaging detectors based on the gas electron multiplier scintillation light *Conf. Record IEEE Nucl. Sci. Symp.* vol 2 829–33

Fraga F A F, Margato L M S, Fetal S T G, Fraga M M F R, Ferreira Marques R and Policarpo A J P L 2001a Optical readout of GEMs *Nucl. Instrum. Methods* A **471** 125–30

Fraga M M R, Bueno C C, Goncalves J A C, Fraga F A F, Ferreira Marques R and Policarpo A J P L 2001b Pressure dependence of secondary NIR scintillation in Ar and Ar/CF_4 *IEEE Trans. Nucl. Sci.* **48** 330–5

Fraga F A F, Margato L M S, Fetal S T G, Ferreira Marques R and Policarpo A J P L 2002a Performance of a tracking device based on the GEM scintillation *IEEE Trans. Nucl. Sci.* **49** 281–4

Fraga F A F, Margato L M S, Fetal S T G, Fraga M M F R, Ferreira Marques R, Policarpo A J P L, Guerard B, Oed A, Manzini G and van Vuure T 2002b CCD readout of GEM-based neutron detectors *Nucl. Instrum. Methods* A **478** 357–61

Fraga M M F R, Fraga F A F, Fetal S T G, Margato L M S, Ferreira Marques R and Policarpo A J P L 2003 The GEM scintillation in He–CF_4, Ar–CF_4, Ar–TEA and Xe–TEA mixtures *Nucl. Instrum. Methods* A **504** 88–92

Hamamatsu 2008 Application note http://sales.hamamatsu.com/

Killenberg M, Lotze S, Mnich J, Roth S, Schulte R, Sobloher B, Struczinski W and Tonutti R 2003 Modelling and measurement of charge transfer in multiple GEM structures *Nucl. Instrum. Methods* A **498** 369–83

Sauli F 1997 GEM: a new concept for electron amplification in gas detectors *Nucl. Instrum. Methods* A **386** 531–4

Seravalli E 2008 A scintillating GEM detector for 2D dose imaging in hadron beams *PhD Thesis* (Amsterdam: IOS) p 47

Seravalli E, de Boer M, Geurink F, Huizenga J, Kreuger R, Schippers J M and van Eijk C W E 2008 A scintillating gas detector for 2D dose measurements in clinical carbon beams *Phys. Med. Biol.* **53** 4651–65

Seravalli E, Hendrikse J, Huizenga J, Kreuger R, Schippers J M, Simon A and van Eijk C W E 2007 First results of a scintillating GEM detector for 2D dosimetry in an alpha beam *IEEE Trans. Nucl. Sci.* **54** 1271–8

Timmer J H, van Vuure T L, Bom V, van Eijk C W E, de Haas J and Schippers J M 2002 A scintillating GEM for 2D-dosimetry in radiation therapy *Nucl. Instrum. Methods* A **478** 98–103